



Paramagnetic magnetostriction in the chiral magnet CrNb₃S₆ at room temperatureMasaki Mito ^{1,2,*}, Takayuki Tajiri,³ Yusuke Kousaka,^{2,4} Yoshihiko Togawa,^{2,4}
Jun Akimitsu,⁵ Jun-ichiro Kishine,^{2,6} and Katsuya Inoue ^{2,7,8}¹Graduate School of Engineering, Kyushu Institute of Technology, Kitakyushu 804-8550, Japan²Chirality Research Center, Hiroshima University, Higashihiroshima 739-8526, Japan³Faculty of Science, Fukuoka University, Fukuoka 814-0180, Japan⁴Graduate School of Engineering, Osaka Prefecture University, Sakai 599-8570, Japan⁵Research Institute for Interdisciplinary Science, Okayama University, Okayama 700-8530, Japan⁶Graduate School of Arts and Sciences, The Open University of Japan, Chiba 261-8586, Japan⁷Graduate School of Science, Hiroshima University, Higashihiroshima 739-8526, Japan⁸Institute for Advanced Materials Research, Hiroshima University, Higashihiroshima 739-8526, Japan

(Received 24 October 2021; revised 25 January 2022; accepted 22 February 2022; published 14 March 2022)

We report that the magnetostriction (MS) effects occur in a paramagnetic state of a chiral magnet CrNb₃S₆. Through a series of experimental tests at room temperature, structural changes were observed at the level of a unit cell. The structural parameters are dependent of the strength and direction of magnetic field (H) even at temperature excessively higher than the magnetic ordering temperature T_c of 127 K. The present paramagnetic MS prominently appeared under $H \parallel$ the ab plane (easy plane) as opposed to under $H \parallel$ the c axis. Features observed in the paramagnetic MS effect significantly differ from those of the spontaneous MS in the vicinity of T_c [Phys. Rev. B **102**, 014446 (2020)]. In this material, the orbital angular momentum L of Cr originates from the hybridization between Cr and Nb, and L is strongly coupled with the crystal structure [Phys. Rev. B **99**, 174439 (2019)]. The present study clarified that the symmetry of the CrS₆ octahedron is sensitive to H even at room temperature. The paramagnetic spin-orbit coupling should induce the distortion of CrS₆ octahedron, resulting in the changes in Cr-Nb($4f$) distance via the change in the hybridization between Cr- a_{1g} and Nb- $4d_{2z}$ orbitals.

DOI: [10.1103/PhysRevB.105.104412](https://doi.org/10.1103/PhysRevB.105.104412)**I. INTRODUCTION**

In systems with strong magnetostructural correlation, the volume of the unit cell changes when the spin system transforms to a certain magnetically ordered state. This phenomenon is termed as “magnetostriction (MS) effect,” and many experimental reports have been published in the fields involving ferromagnetic crystals, alloys, and amorphous alloys [1]. Furthermore, the studies on MS have been enlarged to the first-order transition systems [2], itinerant-electron magnets [3–5], multiferroic systems (perovskite system) including Mn oxides [6–14], heavy fermion systems [15,16], pyrochlore system [17], and lanthanide-iron compounds [18]. Most of the MS effect is related to magnetic ordering and some of MS is related to crystal fields [19,20]. In general, the MS in ferromagnets is phenomenologically interpreted as an effect of magnetoelastic coupling, and it is enhanced with the aid of itinerant electrons. From a macroscopic viewpoint, the aforementioned phenomena can be understood with the point group theory.

The MS in the paramagnetic region is rare: it has been observed in several systems, such as ferromagnetic amorphous alloys, spin liquid [17], and mixed valence manganese oxides [6,8], and it is related to the local moments in the paramagnetic state.

The orbital angular momentum L denotes the exotic physical phenomena via the spin-orbit coupling (SOC) that forms a microscopic manner of magnetostructural correlation. The SOC also brings about magnetocrystalline anisotropy, which in turn can enhance the MS effects. In materials, which belong to Sohncke space group, without rotoinversion symmetry elements [21], the Dzyaloshinskii-Moriya (DM) interaction arises from a combined second-order perturbation of SOC and exchange interaction [22,23]. The competition between exchange interaction and DM interaction stabilizes a long-wavelength helical order, i.e., helimagnetic (HM) order. The magnitude of DM interaction is generally small when compared to the exchange interaction. However, its vector type of interaction is rooted in the crystal structure and governs twisting of spins over the crystal. It brings about nontrivial spin textures such as magnetic superlattice with vortices [24] and kinks [25] at finite magnetic field (H) as well as HM structure at zero H .

The MS effect has been observed in chiral magnets, where the DM interaction can be permitted: for instance, chiral magnets with a B20-type cubic crystal structure allow the existence of multiple DM vectors and the formation of a magnetic vortices lattice called Skyrmion lattice. The H -induced MS, termed forced MS, related to Skyrmion lattice has been studied in MnSi, via the capacitance measurement [26,27]. The relation of MS to the structural symmetry was discussed based on the group theory [27]. In Fe_xCo_{1-x}S with the B20 type structure, the MS at zero H , termed spontaneous

*mitoh@mns.kyutech.ac.jp

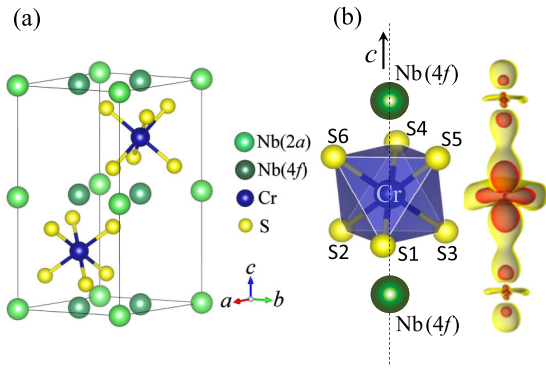


FIG. 1. (a) Crystal structure of CrNb₃S₆. Nb(2a) and Nb(4f) are denoted in light and dark green, respectively. (b) Local structure of CrS₆ octahedron sandwiched with two Nb(4f) atoms and image of hybridization between Cr-*a*_{1g} and Nb-*d*_{z²} orbitals. The following relations hold up: $\angle S1CrS4 = \angle S2CrS5$, $\angle S3CrS6$; $\angle S5CrS6 = \angle S1CrS2$, $\angle S1CrS3$, $\angle S2CrS3$, $\angle S4CrS5$, $\angle S4CrS6$. The two triangles $\Delta S1S2S3$ and $\Delta S4S5S6$ are regular triangles.

MS, has been investigated from the viewpoint of thermal expansion [28].

In 2020, in a typical monoaxial-DM type of chiral helimagnet CrNb₃S₆ with the magnetic ordering temperature T_c of 127 K [29–31], the characteristic spontaneous MS was observed at the boundary between the paramagnetic and HM states [32]: the change in atomic position, reflecting the existence of local distortion, occurs over a wide temperature range up to room temperature. Note CrNb₃S₆ exhibits a strong magnetocrystalline anisotropy on the *ab* plane [33]. Thus the forced MS effect was also observed at the strength of a magnetic field H of 1.2 kOe: a small change in the unit cell volume of 0.4% survives even at room temperature [32].

The crystal structure of CrNb₃S₆ is as follows: Cr³⁺ ions are inserted into the space between hexagonal NbS₂ layers as shown in Fig. 1(a). The insertion of Cr³⁺ does break the inversion symmetry. The material crystallizes as the non-centrosymmetric hexagonal space group $P6_322$ [29,30,34–36]. The Nb positions occupy two sites, 2a and 4f, which are termed as Nb(2a) and Nb(4f) in Fig. 1(a). The Nb(4f) is located so as to get close to the 3S triangle of CrS₆ octahedra as shown in Fig. 1(b). However, in this cluster unit of CrS₆-Nb(4f), the local symmetry with respect to Cr is approximately D_{3d} . Consequently, Cr 3d orbitals lead to an energy splitting of an electron configuration as $t_{2g} \rightarrow e'_g + a_{1g}$. In this case, *a*_{1g} denotes an orbital, $3z^2 - r^2$, that stretches along the *c* axis toward Nb(4f) atoms. The z^2 orbital of Nb(4f) is hybridized with the delocalized *a*_{1g} orbital of Cr [37]. The delocalized *e*'_g orbital of Cr is hybridized with S 3*p* orbitals.

Based on the Lorenz microscopy experiment, a ferromagnetic network develops on the *ab* plane [38] and the magnitude of its intraplane interaction is 140 K [33]. The ESR experiment evaluated the interplane exchange interaction along the chiral *c* axis (16.2 K), the DM interaction (1.29 K), and the easy-plane anisotropy (1.02 K) [39]. The results show fair matching with the values obtained from the

Monte Carlo simulation [33]. Thus the ferromagnetic layer (*ab* plane) with the easy-plane anisotropy stacks along the chiral axis (*c* axis). The magnetization originates mainly from Cr, while the electrical conductivity originates from Nb. For $T < T_c$, prominent magnetoresistance reflecting the change in the magnetic structure was observed [40–42]. We stress that there is a significant cross correlation among chiral structure, chiral magnetic texture, and electric conductivity, because of the orbital hybridization between Cr and Nb(4f). Indeed, the symmetry of CrS₆ octahedron is reduced as the temperature increases above T_c [32]. We are interested in the influence of the symmetry change on the aforementioned cross correlation at room temperature. In this study, to elucidate whether the paramagnetic MS occurs in the microscopic level, we conducted the x-ray structural analysis experiments for CrNb₃S₆ as a function of magnetic field H at room temperature.

II. METHODS

Powders and single crystals of CrNb₃S₆ were synthesized via a chemical vapor transport method, described elsewhere [38]. The powder sample has also been used in the room-temperature x-ray diffraction (XRD) experiment at hydrostatic pressure [30,43] and low-temperature XRD at $H = 0$ [32]. In this study, we performed XRD analyses at room temperature (RT), 299.2 K, using a synchrotron radiation XRD system with a cylindrical imaging plate at the Photon Factory at the Institute of Materials Structure Science, High Energy Accelerator Research Organization [44]. The energy of the incident x rays was 16 keV. Two facing NdFeB magnets (NeoMag Co., Ltd.), product No. N48H with remanence of 13.8 kG and size of $10 \times 6 \times 3$ mm³ and product No. N52 with remanence of 14.5 kG and the size of $10 \times 7 \times 8$ mm³, were located in the aforementioned diffractometer [32]. The H values were changed by controlling the distance between the sample and NdFeB magnets. Then, the H value was always reduced down to zero before constructing new configuration of NdFeB magnets. The experiments for a single crystal of CrNb₃S₆ were conducted in three orientations, $H \perp c$ ($H \parallel ab$ plane), 45° orientation from *c* axis and *ab* plane, and $H \parallel c$. The accuracy of the orientation adjustment was $\pm 2^\circ$. The diffraction spots for single crystals were observed in the vibration mode of every 1° for $\pm 3^\circ$. On the basis of the changes in the spot pattern, the changes in the lattice constants were evaluated. Herein, the atomic positions in the unit cell did not become parameters in the analyses. The pattern of observed diffraction spots depend on the H orientation, such that the error bars depend on both the kind of lattice constant (i.e., *a* or *c*) and the H orientation. In the powder experiments, a series of measurements revealed that the quality of the Debye-Scherrer ring did not change even under H . This in turn suggests the crystallite did not orientate along a specific direction under H . The powder diffraction patterns were analyzed to search how each atomic position changes along with the change in lattice constants by means of the Rietveld refinement using the RIETAN-FP package [45].

The H dependence of magnetization (M) was observed using a commercial superconducting quantum interference device magnetometer to confirm the M values and the magnetic irreversibility between field-cooling and field-warming

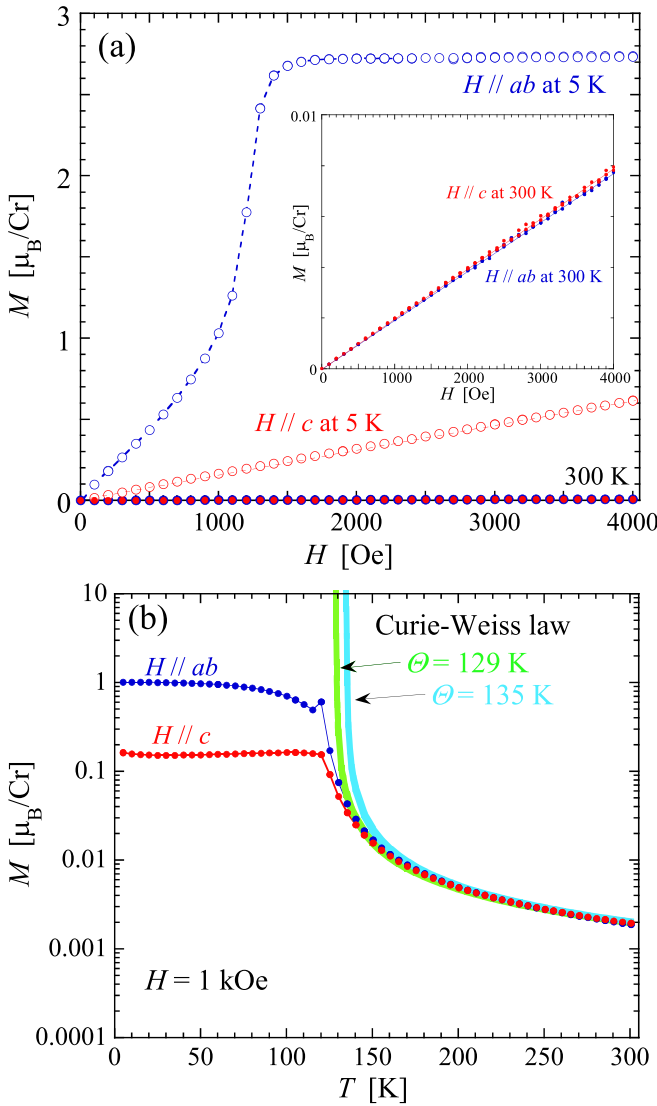


FIG. 2. (a) H dependence of magnetization M for $H \parallel c$ and $H \perp c$ at $T = 5$ and 300 K. The results at 300 K are magnified in the inset. (b) T dependence of M for $H \parallel c$ and $H \perp c$ at $H = 1$ kOe. For reference, the curves representing the Curie-Weiss law with the spin value of $3/2$ and Weiss temperature (Θ) of 129–135 K are also shown. It indicates that there survives ferromagnetic magnetic correlation between spins of CrNb_3S_6 even at 300 K, whereas there is no observable orientation dependence.

processes. The c axis of the single crystal was placed in the direction parallel to H or perpendicular to H . In addition, the electrical resistance R was also observed for $H \perp c$ via the four-terminal method by using a commercial cryostat with a superconducting magnet.

III. EXPERIMENTAL RESULTS

A. Magnetization using a single crystal

Figure 2(a) shows the H dependence of M for $H \parallel c$ and $H \perp c$ at $T = 5$ and 300 K in the H region below 4 kOe. For $H \perp c$ ($H \parallel ab$), M saturates at approximately $3 \mu_B$ at 5 K. For $H \parallel c$, M exhibits a linear increase with respect to

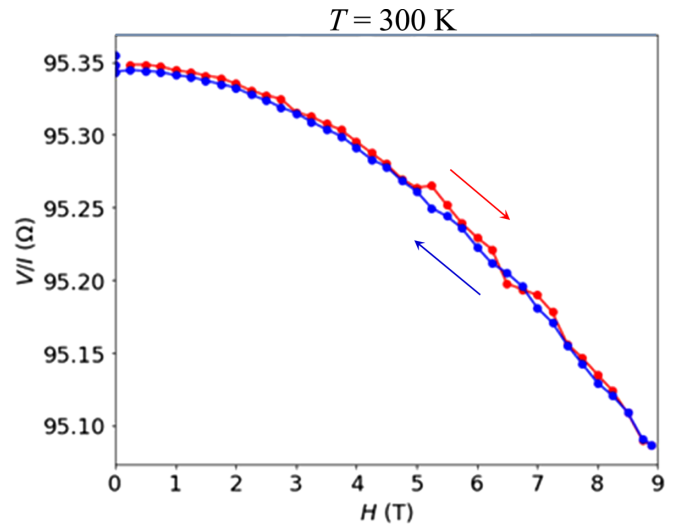


FIG. 3. H dependence of electrical resistance R for $H \perp c$ at 300 K in the processes of increasing H (red) and decreasing H (blue). No hysteresis was observed in the magneto resistance response.

the increase in H . However, at 300 K, the values of M are not dependent on the H direction, as confirmed in Fig. 2(b). The T dependence of M in the paramagnetic region obeys the Curie-Weiss law with the spin value of $3/2$ and positive Weiss temperature Θ of 129–135 K, consistent with the analytic result in Ref. [29]. Even at around 300 K, the Curie law without the Weiss temperature is inappropriate to reproduce the T dependence. Thus, for CrNb_3S_6 , thermal fluctuation of 300 K is not sufficient to eliminate the ferromagnetic magnetic correlation between Cr^{3+} spins on the ab plane.

B. Magnetoresistance using a single crystal

Figure 3 shows the H dependence of electrical resistance R at 300 K for $H \perp c$. In the H region up to 9 T, a 0.2% reduction in R was observed. The spontaneous magnetostriction at $H = 0$ and field-forced magnetostriction at $H = 1.2$ kOe have already been observed over 93–295 K [32]. The magnetoresistance was investigated over 10–160 K [41]. In the present study, we confirmed that the significant effect of the hybridization between the z^2 orbital of $\text{Nb}(4f)$ and delocalized a_{1g} orbital of Cr survives even at 300 K. Given the results of Fig. 2(b), it is important to consider that there the Cr^{3+} spins feeling ferromagnetic correlation trigger the magnetoresistance effect by the conduction electrons of Nb .

C. XRD using a single crystal at RT

In CrNb_3S_6 , the ferromagnetic layer (ab plane) with the easy-plane anisotropy stacks along the chiral axis (c axis). The comparison between the magnetostriction for $H \parallel ab$ plane ($H \perp c$) and that for $H \parallel c$ in the single crystal experiments is a matter of the greatest concern.

Figures 4(a) and 4(b) show the H dependence of normalized lattice constants a and c with those at $H = 0$ for $H \perp c$ at RT. The lattice expands toward the a axis at small fields and the expansion becomes 0.09% at 0.8 kOe. At the same time, the c axis shrinks, which in turn decreases the unit cell volume V as shown in Fig. 4(c). With further increasing H , a

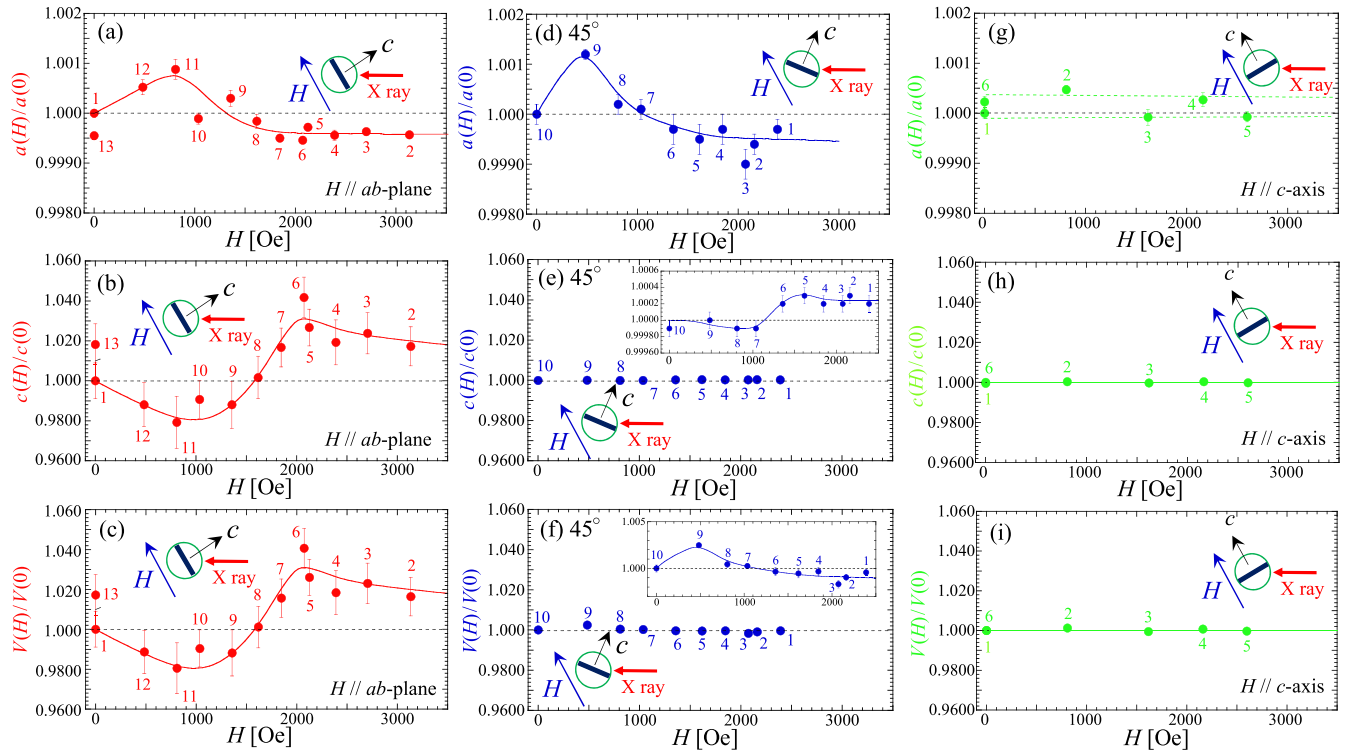


FIG. 4. H dependence of lattice constants, a (a), (d), (g), c (b), (e), (h), and V (c), (f), (i), of CrNb_3S_6 at RT for $H \perp c$ ($H \parallel ab$ plane) (a)–(c), the 45° orientation with respect to c axis and ab plane (d)–(f), and $H \parallel c$ (g)–(i). The numbers adjacent to the symbols denote the sequence of the measurement. The H value was always reduced down to zero before constructing a new configuration of NdFeB magnets, and the numbers denoting the sequence have no important meaning in a series of the H change.

starts to decrease. It becomes smaller than that at $H = 0$ and the shrinkage reaches 0.04%. Conversely, c tends to increase around 1 kOe and it exhibits the 4% expansion at 2 kOe. The 2% expansion remains even above 2.4 kOe, because the value of $c(H)/c(0)$ keeps almost to 1.020. The magnitude of the aforementioned forced magnetostriction is much larger than that of the spontaneous magnetostriction below T_c [32]. Thus the relative change in c is 50 times larger than that in a . Later, the powder experiment shown below yields microscopic information on a correlation of the structural change in the ab plane with that along the stacking direction of the ab plane. Now, we assume that the structural change along the c axis originates from the change in c along the hybridization between z^2 orbital of Nb($4f$) and delocalized a_{1g} orbital of Cr. The change in the unit cell volume V is closely correlated with the change in c . Indeed, their baselines in both c and V exhibit negative slope with respect to H in the considered H region. Hence, in the following, we examine as to whether the aforementioned lattice change occurs in other H orientation.

Figures 4(d)–4(f) show the H dependence of normalized a , c , and V when H is applied along the direction that is 45° with respect to the c axis and ab plane. The entire H dependencies of a and c are similar to those for $H \perp c$ ($H \parallel ab$). First, a exhibits small expansion of more than 0.1% at approximately 500 Oe. The maximum expansion is observed at lower H than that for $H \perp c$. Above 1 kOe, the ab plane shrinks when compared to that at $H = 0$, similar to $H \perp c$. Next, along the c axis, shrinkage and expansion occur similar to that for $H \perp c$, and the switching occurs at 1.2 kOe, which is lower

than that for $H \perp c$. The magnitude of the maximum change in c is at most 0.03%. Quantitatively, the change in a is larger than that in c . The change in V shown in Fig. 4(f) reflects that in a rather than that in c . Thus, by deviating the H direction from the ab plane, the shrinkage and expansion along the c axis is significantly suppressed to the level of one-hundredth.

Figures 4(g)–4(i) show the H dependence of lattice parameters a , c , and V for $H \parallel c$. In the figures, a and c do not exhibit meaningful changes with respect to the change in H . Furthermore, V maintains a constant value.

The comparison among three H orientations in Fig. 4 reveals that the MS occurs when H is applied in a direction parallel to the magnetic easy plane. It is natural to identify any important factors for producing the easy-plane type of magnetic anisotropy. The present MS at RT is observed sufficiently higher than T_c . The order of the easy-plane anisotropy (~ 1 K) as well as the DM interaction (~ 1 K) is much smaller than the thermal energy at RT [39]. Hence it may be worth considering that the paramagnetic MS originates directly from the change in the orbital angular momentum L as opposed to the paramagnetic MS from SOC via spins.

D. XRD using a powder sample at RT

In the case of the powder XRD experiment, the effects of H for all orientations are merged, whereas it is easier to obtain the information on atomic positions than in the single crystal experiment. To elucidate the mechanism at the unit cell level, each atomic position was investigated in the powder x-ray

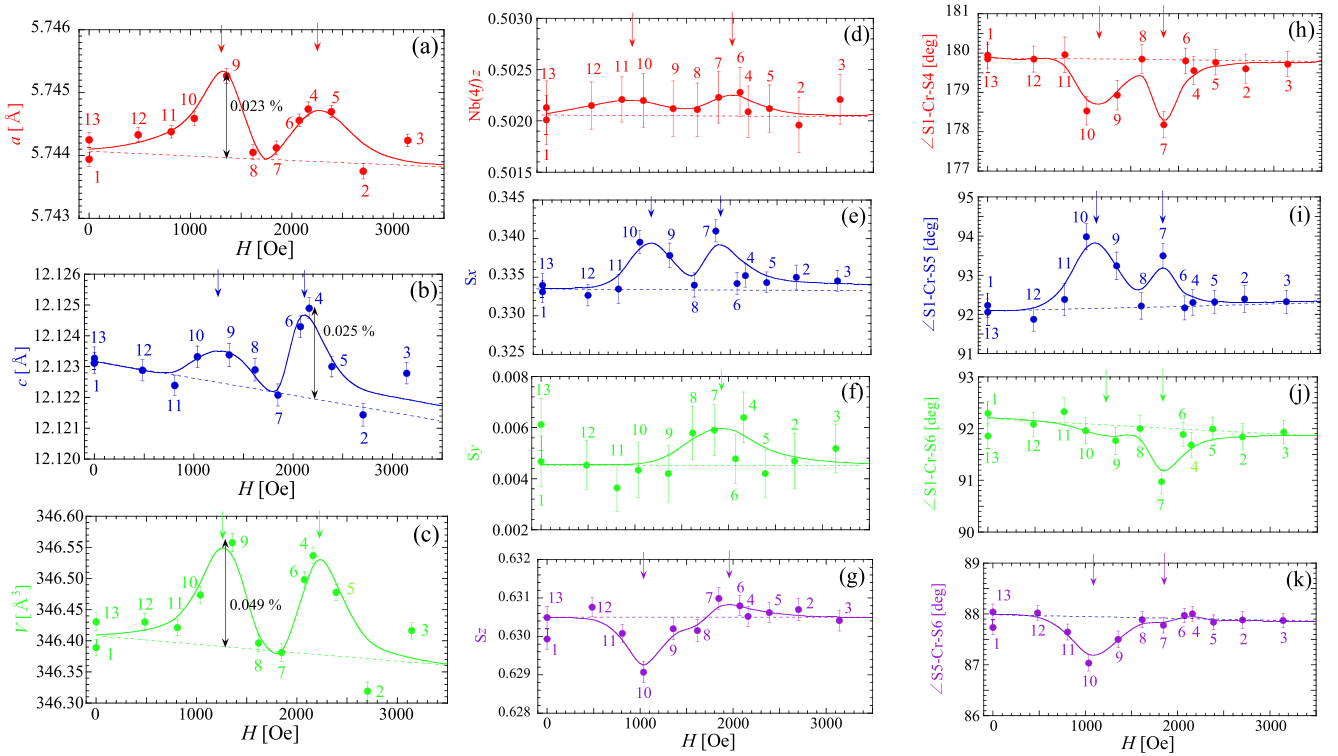


FIG. 5. H dependence of lattice constants [a (a), c (b), V (c)], atomic positions [$\text{Nb}(4f)z$ (d), S_x (e), S_y (f), S_z (g)], and the bonding angles [S1-Cr-S4 (h), S1-Cr-S5 (i), S1-Cr-S6 (j), S5-Cr-S6 (k)], obtained via powder XRD analysis of CrNb_3S_6 at RT. In (a)–(c), for the point with the maximum change, the relative value with respect to the baseline is depicted along with a two-way arrow. The numbers adjacent to the symbols denote the sequence of the measurement. The H value was always reduced down to zero before constructing a new configuration of NdFeB magnets, and the numbers denoting the sequence have no important meaning in a series of the H change. In each figure, characteristic H values are marked with arrows.

analysis experiment. As supplemental data, the results for the powder sample are also shown below.

Figures 5(a) and 5(b) show the H dependence of lattice constants a and c estimated by the powder XRD analysis at RT. They exhibit a double maximum at 1.2–1.3 kOe and 2.1–2.3 kOe. The double maximum in c shifts toward the slightly lower H side than that in a . The location of the maximum in c at 2.1 kOe matches that of the maximum in c of the single crystal for $H \parallel ab$ shown in Fig. 4(b). The maximum in a in the lower H side appears at slightly higher H than the maximum in a of the single crystal for $H \parallel ab$ shown in Fig. 4(a). This behavior is almost consistent with the behavior observed in the experiment for 45° orientation with respect to the c axis and ab plane using a single crystal [see Figs. 4(d)–4(f)]. Comparing the maximum change in $a(H)/a(0)$ [0.023%] and that in $c(H)/c(0)$ [0.025% from the baseline], they are comparable, and both changes are reflected in $V(H)/V(0)$.

Figures 5(d)–5(g) show the H dependence of atomic positions $\text{Nb}(4f)z$, S_x , S_y , and S_z . Specifically, $\text{Nb}(4f)z$ exhibits the maximum at approximately 800 and 2000 Oe. S_x exhibits the maximum at approximately 1200 and 1800 Oe, S_y exhibits the maximum at approximately 1900 Oe, and S_z exhibit prominent minimum at approximately 1000 Oe and tiny hump at approximately 1800 Oe. These changes should be correlated with the change in lattice parameters a , c , and V . Indeed, we found the following correlation among them:

the maximum in a at approximately 1300 Oe and 2250 Oe are related with the change in the lower-side maximum in S_x and the maximum in S_y , respectively. The movement of $\text{Nb}(4f)$ along the z direction (c -axis direction) would be related with a change in the atomic coordinates of S. In this compound, the orbital hybridization between Cr and $\text{Nb}(4f)$ produces an angular momentum L [37]. Hence it is evident that the change in $\text{Nb}(4f)z$ leads to a change in L . The change in atomic coordinates is reflected in the change in the bonding angle, S1-Cr-S4 , S1-Cr-S5 , S1-Cr-S6 , and S5-Cr-S6 , as shown in Figs. 5(h)–5(k). They show characteristic changes at approximately 1200 and 1800 Oe. Specifically, S1-Cr-S4 tends to change far from 180° at two characteristic fields and S1-Cr-S5 , S1-Cr-S6 , and S5-Cr-S6 tend to change far from 90° at two characteristic fields. At approximately 1200 and 1800 Oe, the CrS_6 octahedra tend to be distorted and there the twisting can be enhanced.

IV. DISCUSSION

Figure 6 shows the overview of the change in the twisting of twin CrS_3 tetrahedrons in the process of increasing H , wherein the H region is divided into four regions by focusing five H points. The aforementioned five H points are denoted with blue circles in the two insets of Fig. 6, which present the H dependence of $\angle\text{S1-Cr-S4}$ (a) and $\text{Cr-Nb}(4f)$ (b). Herein, $\angle\text{S1-Cr-S4}$ is one of the characteristic angles for imaging the

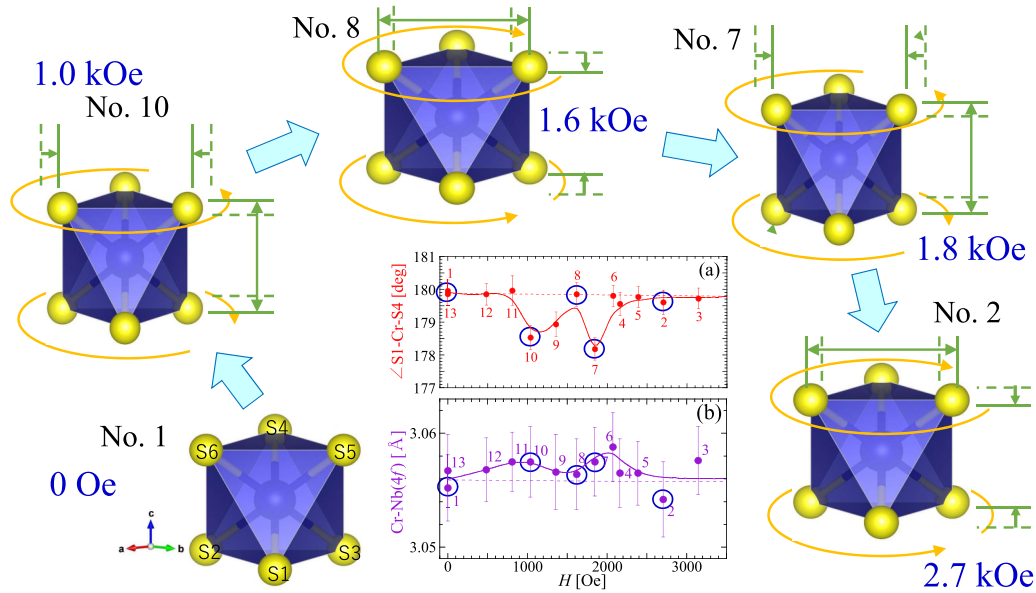


FIG. 6. Overview of the change in the twisting of twin CrS_3 pyramids in the process of increasing H , where the H region is divided into four regions. The number for each structural image corresponds to the sequence number of the experiment using the powder sample. For reference, it is marked with a blue circle in two inset figures, (a) $\angle\text{S1-Cr-S4}(H)$ [it is the same to Fig. 5(h)] that is one of characteristic angles for imaging the twisting of twin CrS_3 tetrahedrons and (b) distance $\text{Cr-Nb}(4f)$ valid for imaging the change in the hybridization between Cr and Nb($4f$) along the z direction (c -axis direction). The green broken lines denote the situation before the change and the solid green lines denote the situation after the change. The orange arrows denote the direction of twisting. In the actual experiment, the measurement sequence was No. 1 \rightarrow 2 \rightarrow 7 \rightarrow 8 \rightarrow 10.

twisting of twin CrS_3 tetrahedrons and the distance $\text{Cr-Nb}(4f)$ is valid for imaging the change in the hybridization between Cr and Nb($4f$) along the z direction.

(1) In the process of 0 \rightarrow 1.0 kOe (No. 1 \rightarrow No. 10), the area of the 3S triangle, ΔS1S2S3 and ΔS4S5S6 , decreases, while the distance between the two 3S triangles increases. The upper inverse pyramid rotates counterclockwise, while the lower pyramid rotates clockwise. The aforementioned change reveals that the strain due to the twisting increases in this process.

(2) In the process of 1.0 \rightarrow 1.6 kOe (No. 10 \rightarrow No. 8), the area of the 3S triangle increases, while the distance between two 3S triangles decreases. Consequently, the relative inverse twisting of two pyramids is released and the strain accumulated in the process of (1) is released.

(3) In the process of 1.6 \rightarrow 1.8 kOe (No. 8 \rightarrow No. 7), structural change similar to that in (1) occurs.

(4) In the process of 1.8 \rightarrow 2.7 kOe (No. 7 \rightarrow No. 2), structural change similar to that in (2) occurs.

Thus the accumulation and release of the twisting-induced strain are repeated. In the actual experiment, the measurement sequence was No. 1 \rightarrow 2 \rightarrow 7 \rightarrow 8 \rightarrow 10. Furthermore, the measurement sequence after No. 2 was not performed in the process of decreasing H systematically; nevertheless, we can consistently see double maximum or double minimum H dependence in most of the figures in Fig. 5. The present H dependence of attractive structural parameters is surely reversible against the increase and decrease in H .

By focusing the CrS_6 octahedra and the hybridization between Cr and Nb($4f$), the changes in the unit cell volume under magnetic field are imaged: the heavy Nb($4f$) atom that moves along the c axis is related with the rotation of the CrS_6

octahedra. This movement brings about a change in a as well as a change in c . Hence it is important to consider “why the aforementioned structural changes occur.”

As the first scenario, we assume that $\text{Cr-}a_{1g}$ orbital can change by SOC via the Cr spins when H is parallel to the ab plane. This leads to the change in a accompanying the distortion of the CrS_6 octahedron. This change in a leads to the change in c through the hybridization between $\text{Cr-}a_{1g}$ and $\text{Nb-}4d_{z^2}$ orbitals. As the second scenario, H directly changes the orbital angular momentum L for Cr, leading to a change in the hybridization between $\text{Cr-}a_{1g}$ and $\text{Nb-}4d_{z^2}$ orbitals. Consequently, the change in the hybridization brings about the change in the unit cell volume.

The characteristic H values for the structural change at RT are observed as identical to the critical H values between CSL-1 and CSL-2 and between CSL-2 and FFM [31]. Theoretically, the former is related to J and D , while the latter is related to J . However, occasional consistency cannot be explained: the magnetic moment at RT is one-thousandth of that below T_c . However, SOC governs the magnetostructural correlation even above T_c ($=127$ K) [32]: even at $H = 0$, the Invar effect, which maintains the constant unit cell volume, is observed below 170 K [32]. With respect to the coordinate of Nb($4f$) and S, significant changes are observed over the wide T range up to RT. In particular, $\text{Nb}(4f)_z$ has the minimum at around 260 K and S_z exhibits large change above T_c . The symmetry of the CrS_6 octahedron is reduced as T increases above T_c [32]. In the present study, the magnetostructural correlation at RT was investigated via the examination of MS. The paramagnetic moment with ferromagnetic magnetic correlation exists even at RT, as seen in Fig. 2(b). The ferromagnetic correlation works on the ab plane and indeed the MS

effects are observed remarkably for the $H \parallel ab$ plane. Herein, the MS cannot be discussed without considering the spin as well as orbital. Therefore, we propose the first scenario—the paramagnetic MS is triggered with SOC. In the future, the first-principles calculations would be desired to understand the paramagnetic magnetostriction at room temperature.

V. CONCLUSION

In this study, we observed magnetostriction in CrNb_3S_6 at room temperature. This intrinsically differs from forced magnetostriction due to the SOC in the vicinity of T_c . The distortion of the CrS_6 octahedron accompanies a change in the hybridization between $\text{Cr-}a_{1g}$ and $\text{Nb-}4d_{z^2}$ orbitals, resulting in the change in the Cr-Nb($4f$) distance. The resultant movement of Nb($4f$) along the z direction leads to a change in the unit cell volume. This is a unique phenomenon of the L -induced structural modulation or small- S -motivated SOC.

The crystal structure can be modified via L . Now, it is an open question as to whether the present paramagnetic MS is triggered from the change in L directly changed by H or from the change in S and the subsequent change in SOC. In this material, the total magnetization at room temperature is quite small due to large thermal fluctuation, whereas the ferromagnetic spin contribution cannot be ignored there. We consider that the present paramagnetic magnetostriction would originate from significant SOC in CrNb_3S_6 .

ACKNOWLEDGMENTS

This study was supported by Grants-in-Aid for Scientific Research, Grant No. (S) 25220803, from the Ministry of Education, Culture, Sports, Science and Technology (MEXT), Japan. This study was also supported by the Centre for Chiral Science at Hiroshima University (the MEXT program for promoting the enhancement of research universities, Japan) and JSPS Core-to-Core Program, A. Advanced Research Networks.

-
- [1] A. Goldman, *Handbook of Modern Ferromagnetic Materials* (Springer Science & Business Media, New York, 1999).
- [2] K. Irisawa, A. Fujita, and K. Fukamichi, *J. Appl. Phys.* **93**, 7266 (2003).
- [3] S. Khmelevskiy and P. Mohn, *Phys. Rev. B* **69**, 140404(R) (2004).
- [4] P. Gegenwart, F. Weickert, R. S. Perry, and Y. Maeno, *Physica B* **378–380**, 117 (2006).
- [5] T. Sakon, Y. Yamasaki, H. Kodama, T. Kanomata, H. Nojiri, and Y. Adachi, *Materials* **12**, 3655 (2019).
- [6] J. M. De Teresa, M. R. Ibarra, J. Blasco, J. García, C. Marquina, P. A. Algarabel, Z. Arnold, K. Kamenev, C. Ritter, and R. von Helmolt, *Phys. Rev. B* **54**, 1187 (1996).
- [7] C. A. Ramos, H. R. Salva, R. D. Sanchez, M. Tovar, F. Rivadulla, J. Mira, J. Rivas, A. M. Lopez-Quintela, L. Hueso, M. Saint-Paul *et al.*, *J. Magn. Magn. Mater.* **226–230**, 582 (2001).
- [8] C. Marquina, M. R. Ibarra, A. I. Abramovich, A. V. Michurin, and L. I. Koroleva, *J. Magn. Magn. Mater.* **226–230**, 999 (2001).
- [9] A. Abramovich, R. Demin, L. Koroleva, A. Michurin, O. Gorbenko, A. Kaul, R. Szymczak, and B. Krzymanska, *Phys. Stat. Sol.* **189**, 907 (2002).
- [10] R. Mahendiran, M. R. Ibarra, C. Marquina, B. Garcia-Landa, L. Morellon, A. Maignan, B. Raveau, A. Arulraj, and C. N. R. Rao, *Appl. Phys. Lett.* **82**, 242 (2003).
- [11] Y. Yamato, M. Matsukawa, T. Kumagai, R. Suryanarayanan, S. Nimori, M. Apostu, A. Revcolevschi, K. Koyama, and N. Kobayashi, *Phys. Rev. B* **78**, 132411 (2008).
- [12] L. I. Koroleva, D. M. Zashchirinskiĭ, T. M. Khapaeva, L. I. Gurskiĭ, N. A. Kalanda, V. M. Trukhan, R. Szymczak, and B. Krzymanska, *Sov. Phys. Solid State* **52**, 96 (2010).
- [13] Y. S. Oh, B.-G. Jeon, S. Y. Haam, S. Park, V. F. Correa, A. H. Lacerda, S.-W. Cheong, G. S. Jeon, and K. H. Kim, *Phys. Rev. B* **83**, 060405(R) (2011).
- [14] Y. Ma, J. Cong, and Y. Sun, *J. Phys.: Condens. Matter* **31**, 205701 (2019).
- [15] P. Morin, J. Rouchy, and G. Creuzet, *J. Magn. Magn. Mater.* **69**, 99 (1987).
- [16] J. Yoshida, S. Abe, D. Takahashi, Y. Segawa, Y. Komai, H. Tsujii, K. Matsumoto, H. Suzuki, and Y. Ōnuki, *Phys. Rev. Lett.* **101**, 256402 (2008).
- [17] J. P. C. Ruff, Z. Islam, J. P. Clancy, K. A. Ross, H. Nojiri, Y. H. Matsuda, H. A. Dabkowska, A. D. Dabkowski, and B. D. Gaulin, *Phys. Rev. Lett.* **105**, 077203 (2010).
- [18] M. M. Abd El-Aal, L. I. Kazokova, V. I. Chechernicov, and A. V. Chermushkina, *J. Magn. Magn. Mater.* **74**, 248 (1998).
- [19] T. Takeuchi, P. Ahmet, M. Abliz, R. Settai, and Y. Ōnuki, *J. Phys. Soc. Jpn.* **65**, 1404 (1996).
- [20] V. M. T. S. Barthem, D. Gignoux, A. Naït-Saada, D. Schmitt, and G. Creuzet, *Phys. Rev. B* **37**, 1733 (1988).
- [21] U. Müller, *Symmetry Relationships between Crystal Structures. Applications of Crystallographic Group Theory in Crystal Chemistry* (Oxford University Press, Oxford, 2013).
- [22] I. Dzyaloshinsky, *J. Phys. Chem. Solids* **4**, 241 (1958).
- [23] T. Moriya, *Phys. Rev.* **120**, 91 (1960).
- [24] A. Bogdanov and A. Hubert, *J. Magn. Magn. Mater.* **138**, 255 (1994).
- [25] Y. Togawa, Y. Kousaka, K. Inoue, and J. Kishine, *J. Phys. Soc. Jpn.* **85**, 112001 (2016).
- [26] M. Matsunaga, Y. Ishikawa, and T. Nakajima, *J. Phys. Soc. Jpn.* **51**, 1153 (1982).
- [27] S. Wang, Y. Hu, J. Tang, W. Wei, J. Cong, Y. Sun, H. Du, and M. Tian, *New J. Phys.* **21**, 123052 (2019).
- [28] K. Shimizu, H. Maruyama, H. Yamazaki, and H. Watanabe, *J. Phys. Soc. Jpn.* **59**, 305 (1990).
- [29] T. Miyadai, K. Kikuchi, H. Kondo, S. Sakka, M. Arai, and Y. Ishikawa, *J. Phys. Soc. Jpn.* **52**, 1394 (1983).
- [30] M. Mito, T. Tajiri, K. Tsuruta, H. Deguchi, J. Kishine, K. Inoue, Y. Kousaka, Y. Nakao, and J. Akimitsu, *J. Appl. Phys.* **117**, 183904 (2015).
- [31] K. Tsuruta, M. Mito, H. Deguchi, J. Kishine, Y. Kousaka, J. Akimitsu, and K. Inoue, *Phys. Rev. B* **93**, 104402 (2016).

- [32] T. Tajiri, M. Mito, Y. Kousaka, J. Akimitsu, J. I. Kishine, and K. Inoue, *Phys. Rev. B* **102**, 014446 (2020).
- [33] M. Shinozaki, S. Hoshino, Y. Masaki, J. Kishine, and Y. Kato, *J. Phys. Soc. Jpn.* **85**, 074710 (2016).
- [34] A. R. Beal, in *Intercalated Layered Materials*, edited by F. A. Levy (D. Reidel Publishing Company, Dordrecht, Holland, 1979).
- [35] F. Hulliger and E. Pobitschka, *J. Solid State Chem.* **1**, 117 (1970).
- [36] L. M. Volkova and D. V. Marinin, *J. Appl. Phys.* **116**, 133901 (2014).
- [37] M. Mito, H. Ohsumi, T. Shishidou, F. Kuroda, M. Weinert, K. Tsuruta, Y. Kotani, T. Nakamura, Y. Togawa, J. Kishine, Y. Kousaka, J. Akimitsu, and K. Inoue, *Phys. Rev. B* **99**, 174439 (2019).
- [38] Y. Togawa, T. Koyama, K. Takayanagi, S. Mori, Y. Kousaka, J. Akimitsu, S. Nishihara, K. Inoue, A. S. Ovchinnikov, and J. Kishine, *Phys. Rev. Lett.* **108**, 107202 (2012).
- [39] D. Yoshizawa, J. Kishine, Y. Kousaka, Y. Togawa, M. Mito, J. Akimitsu, K. Inoue, and M. Hagiwara, *Phys. Proc.* **75**, 926 (2015).
- [40] Y. Togawa, Y. Kousaka, S. Nishihara, K. Inoue, J. Akimitsu, A. S. Ovchinnikov, and J. Kishine, *Phys. Rev. Lett.* **111**, 197204 (2013).
- [41] Y. Togawa, T. Koyama, Y. Nishimori, Y. Matsumoto, S. McVitie, D. McGrouther, R. L. Stamps, Y. Kousaka, J. Akimitsu, S. Nishihara, K. Inoue, I. G. Bostrem, V. E. Sinitsyn, A. S. Ovchinnikov, and J. Kishine, *Phys. Rev. B* **92**, 220412(R) (2015).
- [42] L. Wang, N. Chepiga, D.-K. Ki, L. Li, F. Li, W. Zhu, Y. Kato, O. S. Ovchinnikova, F. Mila, I. Martin, D. Mandrus, and A. F. Morpurgo, *Phys. Rev. Lett.* **118**, 257203 (2017).
- [43] M. Mito, S. Tominaga, Y. Komorida, H. Deguchi, S. Takagi, Y. Nakao, Y. Kousaka, and J. Akimitsu, *J. Phys: Conf. Ser.* **215**, 012182 (2010).
- [44] A. Fujiwara, K. Ishii, T. Watanuki, H. Suematsu, H. Nakao, K. Ohwada, Y. Fujii, Y. Murakami, T. Mori, H. Kawada *et al.*, *J. Appl. Cryst.* **33**, 1241 (2000).
- [45] F. Izumi and K. Momma, *Solid State Phenom.* **130**, 15 (2007).